

PDHA1 Gene Knockout In Human Esophageal Squamous Cancer Cells Resulted In Greater Warburg Effect And Aggressive Features In Vitro And In Vivo

This article was published in the following Dove Press journal:
OncoTargets and Therapy

Lan Liu ¹⁻³
Jing Cao⁴
Jing Zhao⁵
Xiangyu Li⁵
Zhenhe Suo³
Huixiang Li^{1,6}

¹Department of Pathology, School of Basic Medical Sciences, Zhengzhou University, Zhengzhou, Henan Province, People's Republic of China; ²Academy of Medical Science, Zhengzhou University, Zhengzhou, Henan Province, People's Republic of China; ³Department of Pathology, The Norwegian Radium Hospital, Oslo University Hospital, Institute of Clinical Medicine, University of Oslo, Montebello, Oslo, Norway; ⁴Department of Pathology, The Third Affiliated Hospital of Zhengzhou University, Zhengzhou, Henan Province, People's Republic of China; ⁵Department of Oncology, The First Affiliated Hospital of Zhengzhou University, Zhengzhou, Henan Province, People's Republic of China; ⁶Department of Pathology, The First Affiliated Hospital of Zhengzhou University, Zhengzhou, Henan Province, People's Republic of China

Background: One of the remarkable metabolic characteristics of cancer cells is that they prefer glycolysis rather than oxidative phosphorylation (OXPHOS). Pyruvate dehydrogenase E1 alpha subunit (PDHA1) is an important prerequisite for OXPHOS. Our previous studies have shown that low level of PDHA1 protein expression in esophageal squamous cell cancer (ESCC) was correlated with poor prognosis. However, the effect of PDHA1 inhibition on metabolism and biological behavior of esophageal cancer cells remains unclear.

Methods And Results: In this study, a KYSE450 PDHA1 knockout (KO) cell line of esophageal cancer was established by CRISPR/Cas9 technology. Then, the glucose metabolism, cell proliferation and migration abilities, chemotherapeutic tolerance and angiogenesis of the PDHA1 KO cells were investigated in vitro and in vivo. In the PDHA1 KO cells, the glycolysis and the consumption of glucose and glutamine were significantly enhanced, while the OXPHOS was significantly suppressed, implying Warburg effect in the PDHA1 KO cells. Furthermore, it was also proved in vitro experiments that the PDHA1 KO cell obtained proliferation advantage, as well as significantly greater chemotherapy tolerance and migration ability. Xenograft experiments discovered not only larger tumors but also increased angiogenesis in the PDHA1 KO cell group.

Conclusion: Inhibition of *PDHA1* gene expression in human ESCC leads to metabolic reprogramming of Warburg effect and increased malignancies. Targeting ESCC metabolic reprogramming may become a potential therapeutic target.

Keywords: PDHA1, ESCC, Warburg effect, CRISPR/Cas9, xenotransplantation, KYSE450

Introduction

Esophageal squamous cell cancer (ESCC) is a common human malignant tumor, which has a high incidence in some parts of the world.¹ The treatment of ESCC is challenged by chemoresistance, distant metastasis and recurrence.² As cancer cells have their unique metabolic characteristics, increasing attention has been paid to the relationship between abnormal metabolic pathways and malignant behaviors of cancer cells in recent years, and studies in this field may help to disclose promising targets for cancer therapy.³⁻⁵

Compared with normal cells, the overall metabolic framework and pattern of malignant cells have changed significantly, including glucose, amino acids, fatty acids and nucleotide metabolism, which is called metabolic reprogramming.^{6,7}

Correspondence: Huixiang Li
Email lihuixiang99@zzu.edu.cn

Warburg effect is a classical metabolic reprogramming pathway, which means that malignant tumor cells prefer glycolysis even under sufficient oxygen supply, that is, aerobic glycolysis.^{8,9}

Pyruvate dehydrogenase complex (PDHc) plays an important role in oxidative phosphorylation (OXPHOS) by converting pyruvate into acetyl coenzyme A. Inhibition of PDHc activity promotes malignant phenotype and growth of tumor cells, and its low expression level is related to poor prognosis.^{10–13} Pyruvate dehydrogenase E1 alpha subunit (PDHA1) is the key subunit of PDHc, and appropriate expression of PDHA1 is an important prerequisite for OXPHOS. One of our previous studies showed that decreased PDHA1 protein expression in ESCC is associated with poor clinical prognosis.¹⁴ Another study of us suggested that the PDHA1 knockout (KO) in human prostate cancer LnCap cells leads to “Warburg effect”, resistance to chemotherapy, enhanced migration ability and increased expression of stem cell makers.¹⁵

In order to further explore the function of PDHA1 in ESCC, we established a KYSE450 PDHA1 KO cell line by CRISPR/Cas9 technology, and performed a series of experiments in vitro and in vivo, to explore the role of PDHA1 in the metabolic framework and cell biology of esophageal cancer.

Materials And Methods

Cell Lines And Reagents

Esophageal squamous cancer cell line KYSE450 was obtained from ATCC (American Type Culture Collection, Manassas, VA, USA). Cells were cultured in RPMI 1640 (21875-034, Gibco, UK) supplemented with 10% FBS (16000-044, Gibco, USA), 100 U/mL of penicillin and 100 µg/mL streptomycin (15140-122, Gibco, USA) at 37°C and 5% CO₂.

The primary antibodies and drugs used in this study were as follows: PDHA1 (ab 177461, Abcam, Shanghai, People’s Republic of China); ANG2 (bs-0677R, Bioss, Beijing, People’s Republic of China); VEGFRA (GB11034B; Servicebio, Wuhan, People’s Republic of China); P53 (af0879, Affinity Biosciences, USA); Phospho p53 (S15) (ab1431, Abcam, Shanghai, People’s Republic of China); ABCG2 (12-888-42, Invitrogen, USA); CD31 (GB13063; Servicebio, Wuhan, People’s Republic of China); GAPDH (AF5718, R&D Systems, USA); ACTIN (GB12001; Servicebio, Wuhan, People’s

Republic of China); Docetaxel (S1148, Selleckchem, USA); Paclitaxel (S1150, Selleckchem, USA).

PDHA1 KO Cell Line Establishment

Plasmid containing the PDHA1-Cas9/sgRNA vectors targeting to the human *PDHA1* exon1 (Viewsolid Biotech, Beijing, People’s Republic of China) was applied, and the PDHA1-gRNA targeted sequence is ACAGCACGCGG GAGACGGCGG. When reached 50–60% confluence, the cell transfection was performed. The transfection solution consisted of SGRNA, CAS9 and anti-puromycin gene plasmid and liposome 2000. The dosage was 50 µL in each 60 mm dish. The medium was replaced after 24 hrs, puromycin was added after 72 hrs. Forty-eight hours after above, the obtained single cells were placed in 96-well plate for cell cloning. The monoclonal cells were obtained after two rounds of cloning.

Mutation Analysis

Cells were collected and DNA was extracted using a Tissue DNA Kit (D3396-02, OMEGA, USA) following the instructions. Then, the DNA was amplified by PCR (see Table 1 for the sequence of primers). The reaction parameters of PCR were as follows: 98°C lasted for 2 mins for denaturation; 98°C lasted 10 s, 60°C lasted 30 s, 72°C lasted 30 s (35 cycles); 72°C lasted 10 mins. The products were sequenced by Viewsolid Biotech (Beijing, People’s Republic of China).

Western Blot (WB)

Cells were mixed in a RIPA buffer containing protease inhibitors (Thermo SCIENTIFIC, West Palm Beach, FL, USA) and placed on ice for 30 mins to react. Then centrifuged for 5 mins (12,000 rpm) at 4°C to collect the supernatant. Equivalent protein was added to SDS-PAGE gel (10%) for electrophoresis. Then, the protein in the gel was transferred to the PVDF membrane (Thermo SCIENTIFIC, USA) using trans-blot apparatus (Bio-Rad Laboratories Inc, USA). The membrane was blocked in 5% milk (1 hr, room temperature). After blocking, the corresponding primary antibody was added and incubated

Table 1 Primers Of Sequencing

Gene Name		Sequence (5' to 3')
PDHA1	Forward primer	GGACGCCGTTCTGGTTG
	Reverse primer	CTTCCCGTGCCTGTAACCC

overnight at 4°C. Then, secondary antibodies bound by horseradish peroxidase were added (1 hr, room temperature). The membrane immersed in photographic developer (Western Dura Extended Duration Substrate, SuperSignal, USA) was exposed to X-ray film in darkroom.

Immunocytochemistry (ICC), Immunohistochemistry (IHC) And Hematoxylin-Eosin (HE) Staining

Cytoblocks were prepared for ICC. Steps of ICC and IHC were as follows: after dewaxing and hydration, the sections were put into microwave oven for antigen repair (EDTA, PH 9.0). 3% H₂O₂ (25 mins) and 3% BSA (30 mins) were successively used for blocking. The sections were incubated with primary antibody (dilution: PDHA1 1:100, CD31 1:300) (4°C, overnight), then secondary antibody was added and DAB staining was used. HE-staining was prepared as routine.

OCR And ECAR Analyses

The analyses of OCR (cellular oxygen consumption rate) and ECAR (extracellular acidity rate) were carried out using a Seahorse XFe96 Analyzer (Seahorse Bioscience, North Billerica, MA, USA). Cells were inoculated into the XFe96 cell culture microplate at a density of 3×10⁴ cells/well, then overnight to adhere. Before analysis, the medium of the microplate was replaced with new medium consisted of Seahorse XF Base Medium, 10 mM glucose, 2 mM sodium pyruvate and 2 mM glutamine, then the microplate was placed in a CO₂-free incubator for 1 hr before the microplate was transferred to the analyzer. After baseline measurement, oligomycin, FCCP (carbonyl cyanide 4- (trifluoromethoxy) phenylhydrazone) and rotenone/antimycin A were sequentially injected into each well in: 1 μM, 1 μM and 0.5 μM/0.5 μM, respectively, and the real-time OCR and ECAR measurements automatically generated by the system.

Glucose Consumption Assay

The glucose consumption test was carried out with a glucose (GLU) test Kit (end-point method) (C050, Changchun Huili Biotech, Changchun, People's Republic of China). Cells were evenly planted in a 10 cm culture dish. When the confluence reached about 80%, medium was replaced with new (12 mL). Culture medium was taken at 0 hr, 12 hrs and 24 hrs, respectively. Samples were analyzed by an automatic biochemistry analyzer

(Chemray 240, Rayto Life and Analytical Sciences, Shenzhen, People's Republic of China). The wavelength was 510 nm, the determination time was 540 seconds, the sample dosage was 3 μL and the reagent dosage was 300 μL.

Determination Of Glutamine Consumption

The concentration of glutamine in medium was determined by liquid chromatography-mass spectrometry (LC-MS). Sampling method is the same as glucose consumption assay. The experiments were analysed with UltiMate 3000 RS Systems (Thermo Fisher Scientific, People's Republic of China) and a Q Exactive High-Resolution Mass Spectrometer (Thermo Fisher Scientific, People's Republic of China). Firstly, the standard curve of glutamine was drawn by using appropriate amount of standard glutamine and ultrapure water as gradient of different concentration. Sample treatment: 200 μL of 0.2% formic acid/acetonitrile was added to 100 μL of the sample, vortexed and mixed, centrifuged at 15,000 rpm for 10 mins, and the supernatant was sampled and analyzed. Finally, the data were calculated, the glutamine chromatogram collection and integration were processed by software Xcilabur 3.0 (Thermo Scientific, USA), and linear regression was performed with 1/X as the weighted coefficient.

Growth Curve Analyses

Cell suspension was inoculated into a 96-well plate (3000 cells/well). After cell adherence, the plate was transferred to Incucyte FLR Cell Imaging System (Essen Biosciences, UK) for 72 hrs. Set to image once every 3 hrs, 2 frames per well. Cell growth curve was drawn using the corresponding software installed in the InCucyte System. The final cell proliferation curve was fitted by statistical calculation of three parallel experimental results.

Cell Cycle Analysis

Cells were collected and centrifuged to obtain cell precipitation. 75% ethanol (pre-cooled at -20°C) was added to the cell precipitation, then stay overnight at 4°C. After washing and suspending the cells with PBS, 2 μL RNase A (1 mg/mL of deionized water) was added to remove the RNA, then bath at 37°C for 40 mins. 100 μL PI (concentration 100 g/mL, PBS preparation) staining solution was used for 20 mins. Cell cycle was measured by BD LSRII

Flow Cytometer (BD Biosciences, USA) and the results were analyzed by Modfit Software (Verity Software House, USA).

Chemosensitivity Assays

The cells were evenly planted into the 60 mm dishes (800 cells/dish). Randomly grouped after adherence, different concentrations of chemotherapy drugs (docetaxel 0.25nM, docetaxel 0.5nm, paclitaxel 1nm, paclitaxel 2nm) were added into the dishes and cultured for 9 days. Then, the dishes were fixed with 4% polyformaldehyde, and stained with 0.1% (w/v) crystal violet in methanol. Colony counting was done after the dish was dried.

Wound Healing Assay

The cells were evenly planted on the 6-well plate (5×10^5 cells/well), when the cell fusion degree reached 90%, each well was scratched with the pipette tips, washed with PBS, then serum-free medium was added. The plate was put into the incubator and take pictures every 12 hrs. Adobe Photoshop software was used to calculate the healing width.

Transwell Cell Migration Assay

700 μ L medium containing 10% FBS was added to a 24-well plate, the transwell chamber (8 μ m pore size, Corning 3422, USA) was placed on the medium. 200 μ L of the cell suspension (1×10^6 /mL, with serum-free medium) was added in the upper room, then the plate was placed in the incubator. After 48 hrs, the chamber was washed and fixed in methanol, stained with 1% crystal violet for 30 mins. The number of migrating cells was counted by microscopy.

Transcriptomic Analysis

Transcriptome sequencing was performed at BGI (Shenzhen, People's Republic of China). Procedures: the total RNA was isolated using mRNA enrichment or rRNA depletion methods. Purified RNA was fragmented by interrupting buffer, retranscribed to the DNA chain with random primers, synthesized double-stranded DNA. Flatten the end of the double-stranded DNA, phosphorylate the 5' end and form a sticky end protruding from A at the 3' end, connect a bubbling joint with protruding T at the 3' end. After PCR amplification, the conjugates were heated and denatured into single chains. A single-stranded cyclic DNA library was constructed by cyclization of single-stranded DNA with a bridge primer. DNA nanospheres

(DNB) were obtained by rolling circle replication (RCR), and the fluorescence signal was amplified. DNB was loaded into pattern nanoarray and read, sequenced and analyzed on BGIS EG-500 platform.

RT-PCR

RNA was extracted by TRIzol Reagent (Ambion, life technologies, Carlsbad, California, USA), concentration and purity of RNA were measured by Nanodrop 2000 (Thermo Science, USA). RevertAid First Strand cDNA Synthesis Kit (K1622, Thermo Scientific, USA) was used to synthesize the cDNA (see Table 2 for the sequence of primers). FastStart Universal SYBR Green Master (Rox) (Roche, Mannheim, Germany) was used for quantitative real-time PCR in StepOnePlus Real-Time PCR System (Thermo Fisher Scientific). The parameters of PCR were: 95°C lasted 10 mins, 40 cycles (95°C lasted 15 s and 60°C lasted 60 s). The results were processed by using $2^{-\Delta\Delta Ct}$.

Mouse Xenotransplantation

Animal experiments were approved by the Ethics Committee of the First Affiliated Hospital of Zhengzhou University. The guidelines followed for the welfare of the animals is: National standard of the People's Republic of China GB/T 35892-2018, Laboratory animal – Guideline for ethical review of animal welfare. Ten Balb/c male nude

Table 2 Primers Of RT-qPCR

Gene Name		Sequence (5' to 3')
IL32	Forward primer	AGGACGACTTCAAAGAGGGCTAC
	Reverse primer	CTCGGCACCGTAATCCATCTC
IL1A	Forward primer	AACCAGTGCTGCTGAAGGAGAT
	Reverse primer	GTTTGGATGGGCAACTGATGTG
IL1RL1	Forward primer	CCTCTACAACTGGACAGCACC
	Reverse primer	GGGCTCCGATTACTGGAAACA
CCL20	Forward primer	CACAGACCGTATTCTTCATCCTAAA
	Reverse primer	CTTTTTTACTGAGGAGACGCACAA
GPR31	Forward primer	GTGCTGTTTGTCTGTGCTTTC
	Reverse primer	GCCCGTGACATCCGAGGTAT
INHBA	Forward primer	GGAGGGCAGAAATGAATGAACCT
	Reverse primer	CTCTCCGAGCGTCTACTACTTTT
BDKRB2	Forward primer	TGTTCTGTGAGGACTCCGTGC
	Reverse primer	CAGAAGACGCTGAGGACAAGAT
ANXA10	Forward primer	GGTCCTATGGGAAGCCTGTC
	Reverse primer	CCTTATGGTCAGCAGGTCTATTTT
IL24	Forward primer	TCACTTACAGGACCAGAGGGACA
	Reverse primer	AGGGTCTGCTGGCTAAAGTCC
CSF2	Forward primer	AGCCTCACCAAGCTCAAGGG
	Reverse primer	CTGGGTTGCACAGGAAGTTTC

mice (4–5 weeks, 18±2 g) were purchased from Beijing Vitalriver Laboratory Animal Technology (Quarantine Certificate Number: 11400700315832, Beijing, People's Republic of China). The mice were randomly divided into groups, labeled and weighed. Cells were collected and adjusted to 5×10^7 /mL in serum-free medium. After sterilizing the right subaxillary skin of mice, 100 μ L cell suspension was injected into the subcutaneous. The growth of tumors was observed daily, and the body weight was measured twice a week. On the 25th day after inoculation, the tumor volume ($V = \text{longer axis} \times \text{shorter axis of the tumor} / 2$) reached 2000 mm³, and the experiment was terminated. The mice were killed and the tumors were collected for subsequent experiments.

Detection Of MVD

Microvessel density (MVD) was evaluated by IHC of CD31. Criteria for microvessel identification: complete lumen and red blood cells are not required, as long as there is obvious staining of vascular endothelial cells and they can be separated from adjacent vessels, tumor cells and interstitial components, they are considered as independent vessels; excluding vessels with thick muscular layer. The mean vessel number of six random regions (200-fold) was calculated as MVD (number/HP). Analysis software: Image-pro plus 6.0 (Media Cybernetics, Rockville, MD, USA).

Flow Cytometry

Cells were collected and washed with PBS at 4°C, then centrifuged to obtain cell precipitation. After shaking and mixing, the cells were labeled with 100 μ L ABCG2 (ATP-binding cassette super-family G member 2) direct-labeled antibody (5 μ L (0.25 μ g)/test) and stained for 30 mins in dark. After the cells were washed and suspended with PBS, the appropriate channels were selected according to the fluorescent dyes on the antibody for detection. The positive rate of cells and the average fluorescence intensity of positive areas were analyzed by FlowJo software.

Statistical Analyses

GraphPad prism 7.0 was used for statistical analysis. The analysis methods were one-way ANOVA or Student's *t*-test. All data were repeated at least three times. The results were shown as means±SEM, and $P < 0.05$ was considered statistically significant.

Results

PDHA1 Gene KO KYSE450 Cell Line Characterization

A KYSE450 *PDHA1* gene KO cell line (KYSE450 PDHA1 KO) was established by using CRISPR/Cas9 technology. The sgRNA used in this study resulted in a 34-base deletion in one allele of the first exon, which created an early terminator “TAG” shortly after this mutation. The WT and the mutation sequences are shown in Figure 1A and B. ICC and WB were used to confirm the PDHA1 KO status, which verified that the PDHA1 protein expression was negative in the KYSE450 PDHA1 KO cells while positive in control cells (Figure 1C and D).

PDHA1 KO Caused Metabolic Reprogramming In The KYSE450 Cells

To investigate the metabolic profile of PDHA1 KO cells, OCR and ECAR were measured both under basal conditions and under the application of oligomycin, FCCP and rotenone/antimycin A. OCR was used to measure OXPHOS and ECAR as a instruction of glycolysis. The basal OCR of the PDHA1 KO cells was 101.67 ± 27.30 pmol/min per 3×10^4 cells, which was much lower than the parental cells (147.33 ± 5.69 pmol/min, $p = 0.047$, Figure 2A and B). At the stressed condition induced by FCCP, the parental cells acted out a concomitant OCR increase (33.33 ± 1.53 pmol/min), while the increasement of the PDHA1 KO cells was much smaller (1.00 ± 1.73 pmol/min) ($p = 0.000$, Figure 2A and B). These data indicated that the reserve respiratory capacity of the PDHA1 KO cells was significantly reduced, meaning that the PDHA1 KO cells already lost the ability to hold both basal OCR and OCR induction under stress condition.

However, the PDHA1 KO cells presented much higher level of basal ECAR (57.60 ± 3.58 mpH/min) than the parental cells (32.12 ± 2.31 mpH/min, $p < 0.0001$) (Figure 2C and D). Oligomycin is an inhibitor of ATP synthase, its application forces cells to shift OXPHOS to glycolysis, therefore maximum cellular ECAR can be revealed. After injection of oligomycin, the PDHA1 KO cells kept almost the same level as the basal ECAR (63.45 ± 6.54 mpH/min), while parental cells had a remarkable increasement (up to 57.12 ± 3.65 mpH/min, $p = 0.000$) (Figure 2C and D). These data indicated that the glycolytic reserve capacity of the PDHA1 KO cells was significantly reduced, implying a constant higher level of ECAR, or increased glycolysis in the PDHA1 KO cells.

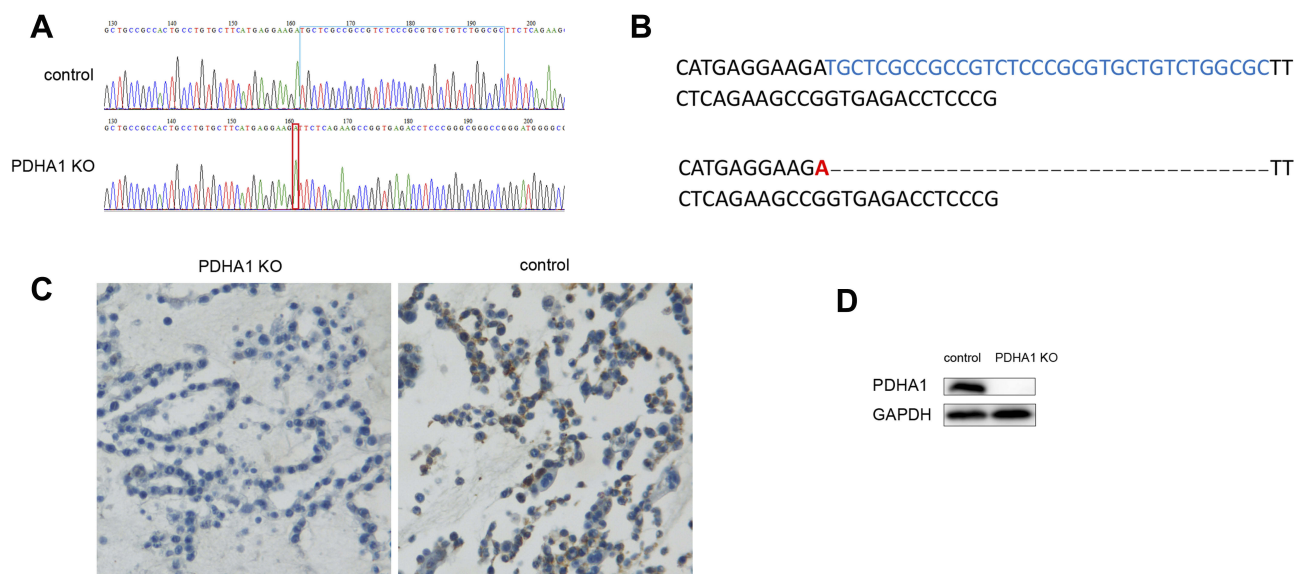


Figure 1 Mutation identification and protein expression verification in the PDHA1 KO cells.

Notes: (A, B) Representative sequencing charts and sequences of PDHA1 PCR products, respectively. The upper panels show the control sequence chart or sequence in the KYSE450 cells while the lower panels are the mutated sequence chart or sequence detected in the PDHA1 KO cells, respectively. The part surrounded by blue box in A or marked in blue in B is the starting deletion base or the deleted 34 base, which happened in PDHA1 KO cells marked in red, respectively. (C, D) ICC and WB analysis of PDHA1 expression, respectively, where PDHA1 protein expression in the PDHA1 KO cells is negative while its expression in the control cells is positive.

The glucose and glutamine consumption tests verified that the PDHA1 KO cells consumed significantly more glucose ($p < 0.001$ at 12 hrs, $p < 0.001$ at 24 hrs) and glutamine ($p < 0.05$ at 12 hrs, $p < 0.001$ at 24 hrs) than the parental cells (Figure 2E and F). These results suggested that the PDHA1 KO cells consumed more glucose and glutamine to compensate energy metabolism, which results in enhanced glycolysis and glutaminolysis and decreased OXPHOS in these cells.

PDHA1 KO KYSE 450 Cells Obtained Cell Proliferation Advantage

To investigate the effect of *PDHA1* gene KO effect on cell proliferation, cell proliferation tests and cell cycle analysis were carried out. The growth curves analyses disclosed that the growth of the PDHA1 KO cells was significantly faster than the parental cells in vitro (Figure 3A and B). Compared with the parental cells, the PDHA1 KO cells held increased percentage of S phase ($p < 0.001$) and decreased percentage of G1 and G2/M phase ($p < 0.001$) (Figure 3C and D).

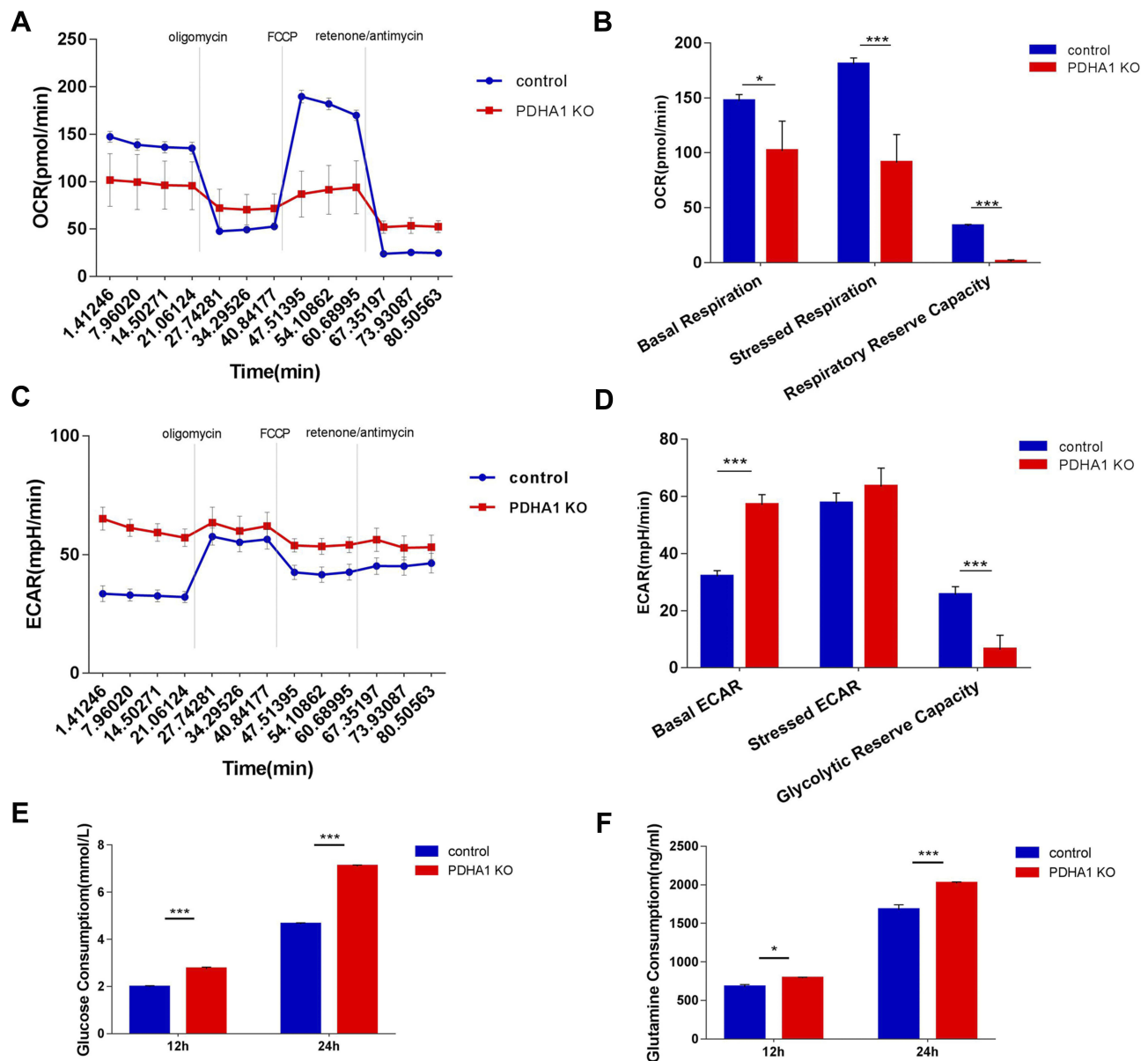
PDHA1 KO Resulted In Chemotherapy Resistant

To analyze the effect of PDHA1 KO on the chemoresistance in the KYSE450 cell line, we performed colony

formation experiments with different concentrations of docetaxel (DOC) and paclitaxel (PAC) after preliminary dose optimization experiments. As shown in Figure 4A and B, compared to the parental cells, there are significantly more PDHA1 KO cells survived in both 0.25nM and 0.5nM docetaxel treatments ($p < 0.001$). Corresponding inhibition rates were calculated as shown in Figure 4C, showing that the inhibition rate in the KO group was significantly lower ($p < 0.001$ at 0.25nM, $p < 0.01$ at 0.5nM). The results of paclitaxel (1nM and 2nM) are similar to those of docetaxel, and the corresponding images are shown in Figure 4D–F. These data suggested that PDHA1 KO cells were more resistant to both docetaxel and paclitaxel than the parental cells.

PDHA1 KO Cells Were Significantly Highly Migratory

The effect of PDHA1 KO on cell migration ability was examined using a wound healing test and a transwell migration assay. As shown in Figure 4G and H, the wound healing rate of the KO cells was significantly faster than the control groups, both at 24 hrs ($p < 0.01$) and 36 hrs ($p < 0.01$). Transwell cell migration assay showed that the PDHA1 KO cells had significantly greater migration capacity (Figure 4I and J, $p < 0.001$). These experiments suggested that in the KYSE450 cell



line, PDHA1 KO resulted in a significantly higher cell migration ability.

Transcriptomic Analysis

In order to explore the difference of transcriptome between the PDHA1 KO cells and parental cells, we carried out transcriptomic analysis. Attention was specially paid so that culture condition and cell density of two groups were comparable. The scatter plot of differentially expressed genes (DEGs) distribution is shown in Figure 5A.

Compared with parental cells, a total of 1803 up-regulated genes and 862 down-regulated genes with significant statistical significance (under the criteria of a minimum twofold change and a $P<0.05$) were detected. Then, we performed a pathway enrichment analysis of DEGs based on Kyoto Encyclopaedia of Genes and Genomes (KEGG) database. As shown in Figure 5B and C, pathways in cancer were the most influenced pathways. Then, we presented the most differentially expressed genes by heat map (Figure 5D). Nine of the most significantly up-regulated genes (*CSF2*,

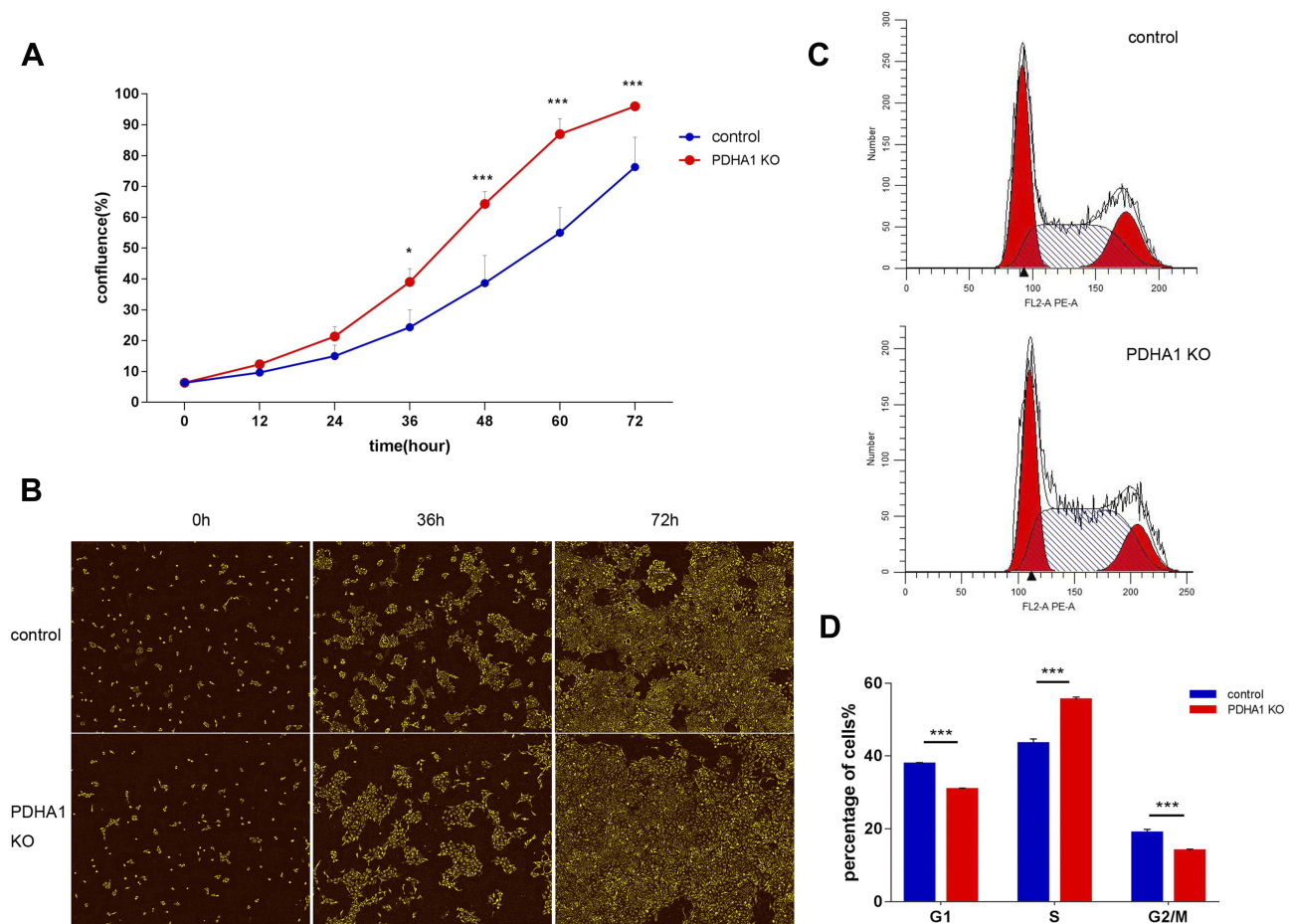


Figure 3 Effect of PDHA1 KO on cell proliferation and cell cycle.

Notes: (A, B) Representative growth curves and images, respectively. (C, D) Representative flow cytometry figures and the corresponding histograms, respectively. The histograms represent the percentage of the PDHA1 KO cells and parental cells in the G1, S and G2/M phases. (* $P < 0.05$, *** $P < 0.001$).

ANXA10, *INHBA*, *IL1RL1*, *IL32*, *CCL20*, *IL1A*, *GPR31*, *BDKRB2*) associated with tumor were selected and verified by RT-qPCR (Figure 5E), and the results were consistent with the transcriptome analysis.

PDHA1 KO Promoted Tumor Growth And Angiogenesis In Nude Mice

To evaluate the effect of the PDHA1 KO on tumor growth in xenograft model, we injected the PDHA1 KO cells and control cells subcutaneously in nude mice, the observation lasted for 25 days (Figure 6A and B). Compared with the control group, the average tumor weight was heavier (Figure 6C), and the average tumor volume was significantly bigger in the PDHA1 KO group ($P < 0.01$, both in day 23 and day 25) (Figure 6D), indicating PDHA1 KO cells had growth advantage in nude mice. However, despite the heavier tumor weight, the body weight of the

PDHA1 KO mice was lighter, which meant that these mice were in worse physical condition (Figure 6E).

HE staining was performed on the xenograft tumor tissues, respectively (Figure 6F). Histologically, tumor cells in the PDHA1 KO xenografts were rather poorly differentiated, disorderly arranged with various cell morphology, higher nucleo-cytoplasmic ratio, and rather visible nucleoli. Although areas with rather well-differentiated tumors cells could also be seen in relatively regular patterns, and sometimes with nest-like distribution in the PDHA1 KO cell xenograft tumors, the control xenograft tumors showed relatively rather visible keratinized pearls.

Vascular proliferation in tumor tissue reflects its ability to induce angiogenesis, and the tumor MVD is usually taken as an indicator of tumor angiogenesis. To explore the effect of PDHA1 KO on tumor angiogenesis, we calculated MVD of each group by counting the number of the microvessels per high-power field (hpf) in the

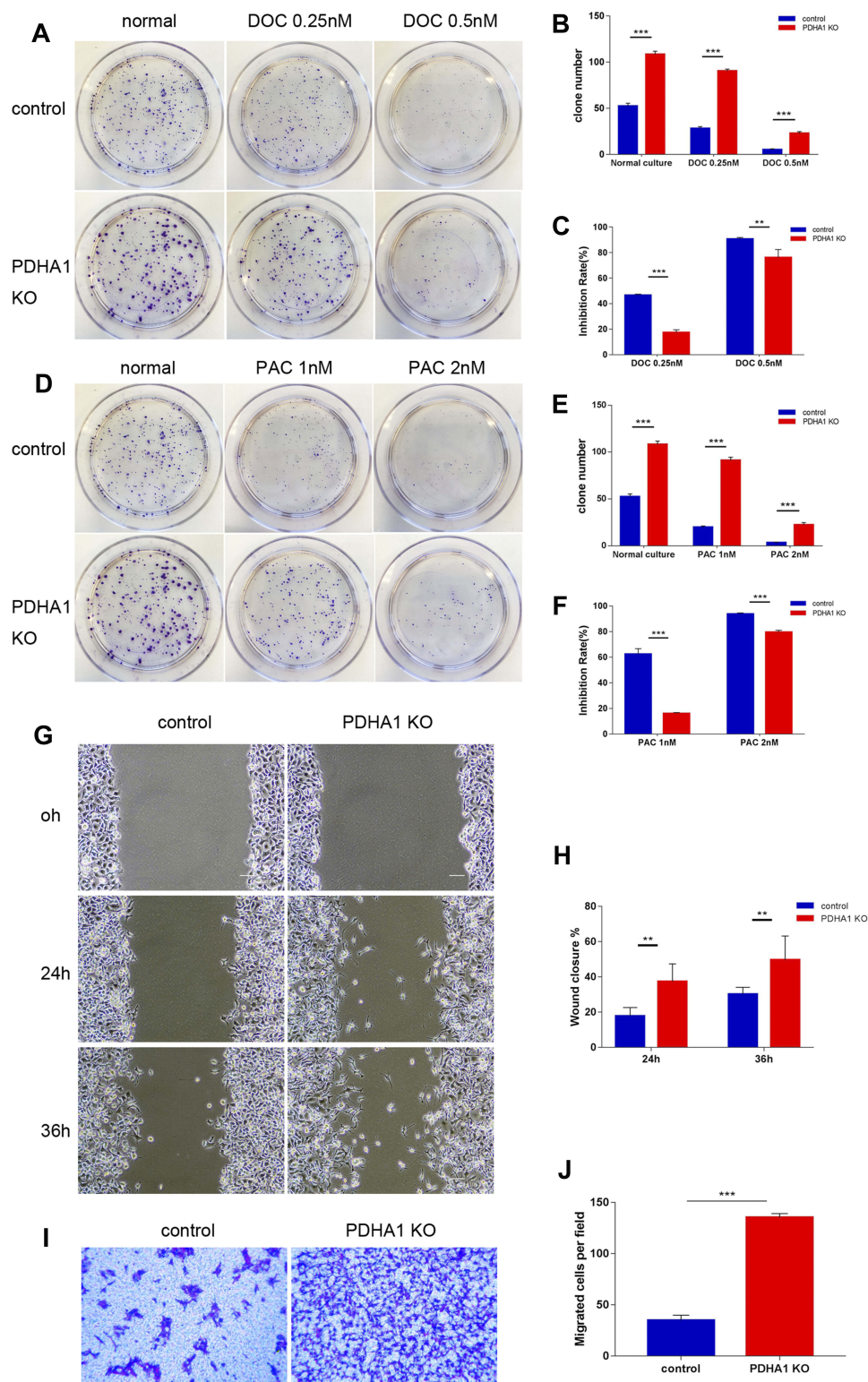


Figure 4 Enhanced chemotherapy-resistant and migration ability in the PDHA1 KO cells.

Notes: Photos of colony formation assay of docetaxel (DOC) results are shown in (A), and the corresponding clone number histograms and colony formation inhibition rate (clone number in the dish without drug minus clone number in the dish with drug) divided by clone number without drug are shown in (B, C), respectively. Photos of colony formation assay experiment of paclitaxel (PAC) are shown in (D), and the corresponding clone number histograms and colony formation inhibition rate are shown in (E, F), respectively. Representative wound healing images are shown in (G), and the corresponding histograms are shown in (H). Transwell assay images are shown in (I), and the corresponding histograms are shown in (J). (**P<0.01, ***P<0.001).

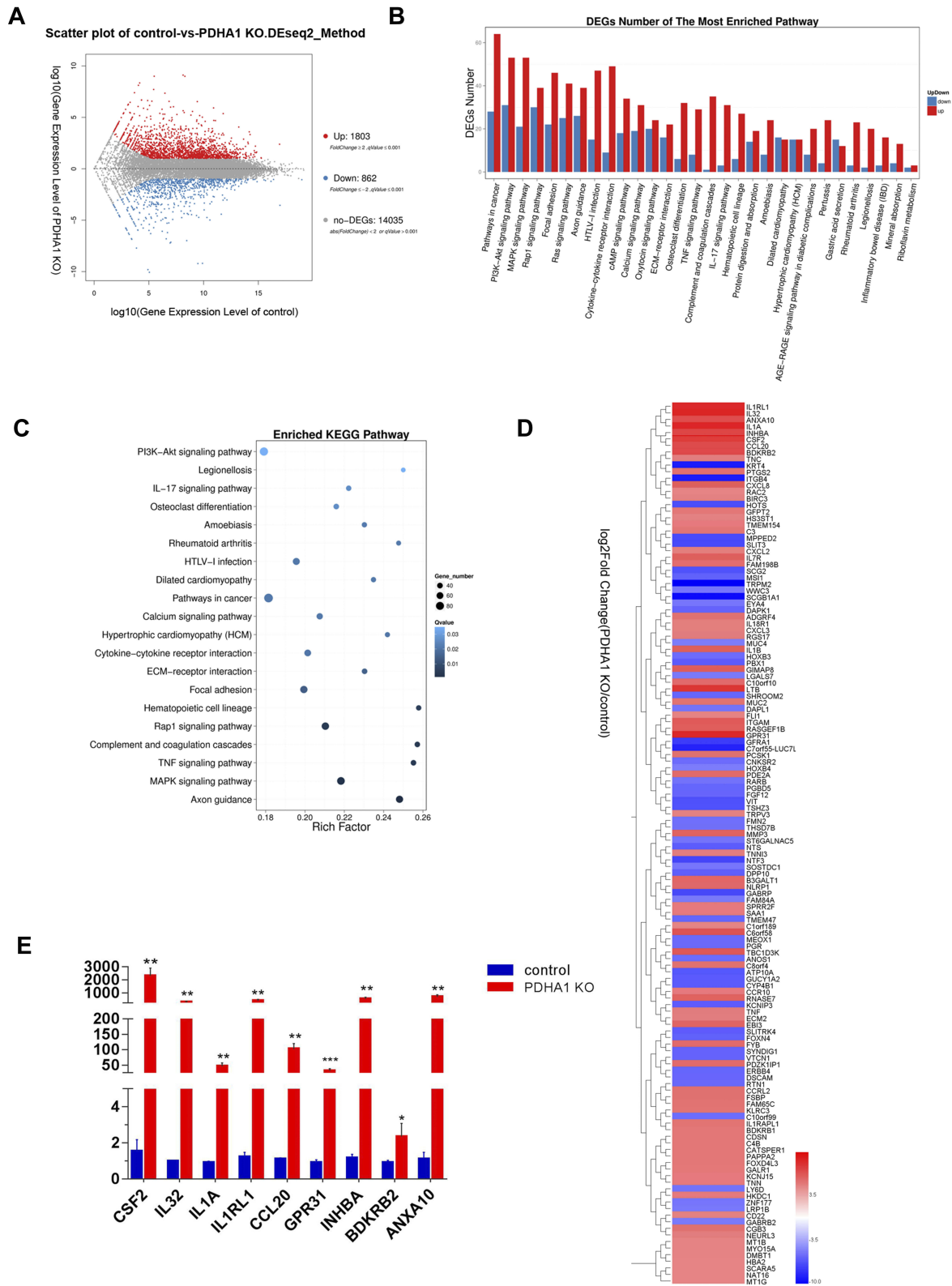


Figure 5 Transcriptome sequencing results. **Notes:** (A) Scatter plots of all expressed genes by BGISEQ-500 (parental-vs-KO). Blue plots are down-regulated genes, the red ones are up-regulated genes, grey ones represent to no statistical significance changing genes. (B) DEGs numbers of the most enriched pathway. (C) Enriched KEGG pathways presented by rich factor (calculated by gene number and Q-value). (D) Most prominent differentially expressed up-and-down genes, \log_2 fold change (KO/parental). (E) Top nine up-regulated tumor-related genes verified by RT-qPCR. (* $P < 0.05$, ** $P < 0.01$, *** $P < 0.001$).

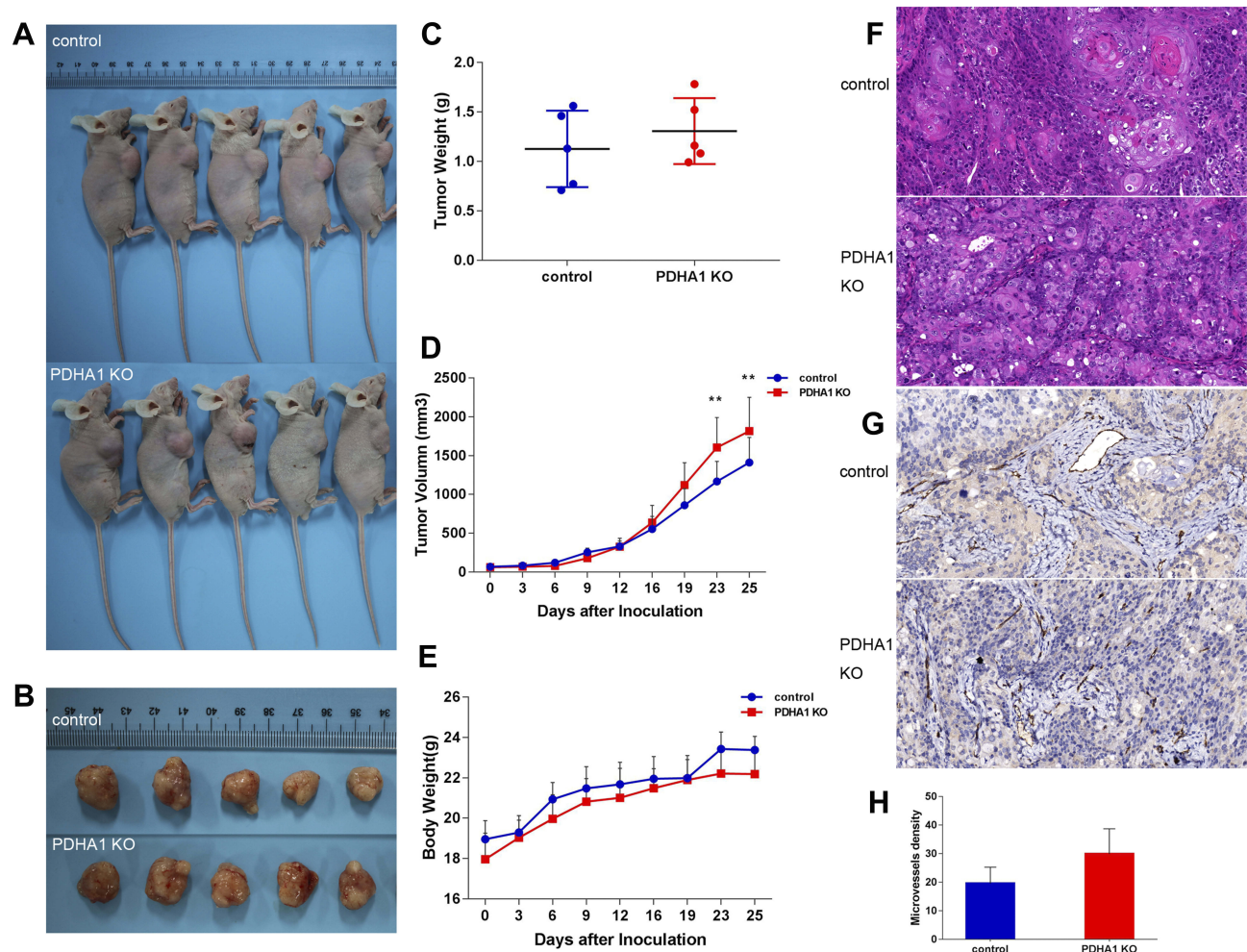


Figure 6 PDHA1 KO promoted tumor growth and angiogenesis in nude mice.

Notes: (A) Representative images of mice with xenograft tumors derived from the PDHA1 KO and control cells subcutaneously. (B) The tumors removed from the mice at the end of the experiment. The tumor weight, tumor volume and the mice body weight of the two groups are shown in (C–E), respectively. Representative HE slide pictures from both groups are shown in (F), where the keratinized pearl areas were less prominent in the PDHA1 KO mouse slide than that in the control mouse slide ($\times 400$). (G) A representative CD31 IHC image ($200\times$), where the blood vessels in tumor tissues were stained in yellow brown, and the histograms of MVD counting in both groups are shown in (H) ($P=0.0583$). (** $P<0.01$).

section with an antibody reactive to CD31 (Figure 6G). Compared with the control group, the MVD value in the PDHA1 KO group was higher (Figure 6H).

PDHA1 KO Cells Resulted In Higher Expression Of Malignant Markers

In order to analyze the relevant molecular mechanisms, we examined some factors related to cell proliferation, angiogenesis and drug resistance. Compared with the control cells, the protein expression of P53 and phosphorylated P53 (S15), angiopoietin-2 (ANG2) and vascular endothelial growth factor A (VEGFA) were significantly increased in the PDHA1 KO cells (Figure 7A and B). The expression of ABCG2 surface antigen examined by flow

cytometry showed that the expression of ABCG2 in the PDHA1 KO cells was significantly higher than the control group (Figure 7C).

Discussion

Metabolic reprogramming is essential for the survival and proliferation of cancer cells. Abnormally active metabolic pathways allow cancer cells ingest large amounts of nutrients, to produce ATP, prepare precursors for proliferation, and also to tolerate adverse environments. Reprogrammed metabolic pathways have become an important target for cancer therapy in recent years.¹⁶ Inhibition of activated metabolic activity can inhibit the proliferation of tumors.¹⁷ Drugs that target specific metabolic processes have been

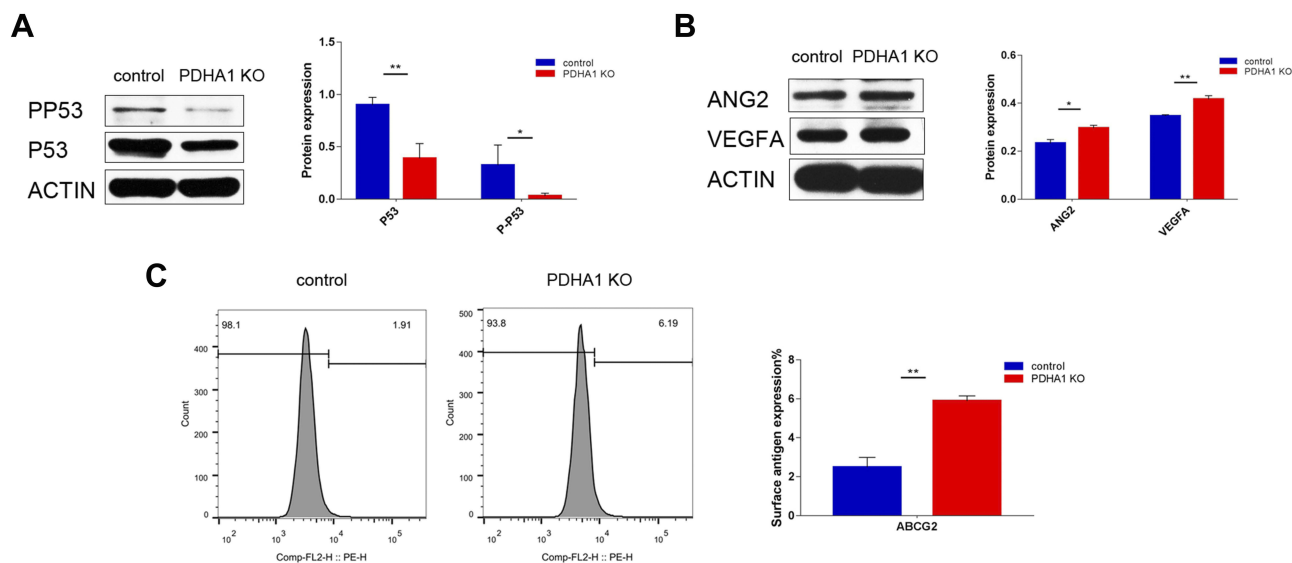


Figure 7 Expression of malignant markers.

Notes: Decreased P53 and phosphorylated P53 (S15) protein expressions in the PDHA1 KO cells are shown in (A) at the left, and the corresponding histograms are shown at the right. Increased ANG2 and VEGFA protein expressions in the PDHA1 KO cells are shown in (B) at the left, and the corresponding histograms are shown at the right. Representative flow cytometry figures of ABCG2 detection are shown in (C) at the left, and the corresponding histograms are shown in (C) at the right, where significantly upregulated ABCG2 is seen in the PDHA1 KO cells. (* $P < 0.05$, ** $P < 0.01$).

used in tumor therapy, such as asparaginase inhibitors for the treatment of acute lymphoblastic leukemia.¹⁸

The Warburg effect was discovered nearly a century ago and exists in a variety of cancer cells. Studies on embryonic stem cells (ESCs), hematopoietic stem cells (HSCs), mesenchymal stem cells (MSCs) and induced pluripotent stem cells (iPS) have found that these cells perform with dynamic glycolysis and inhibited OXPHOS, which is considered to be an important factor in maintaining cell stemness.^{19–23} It was also found that the glycolysis ability of highly malignant cancer cells was stronger than that of low malignant cancer cells, and Warburg effect was related to the malignant behavior of cancer cells.^{24–26}

PDHc consists of three enzymes and a binding protein, namely pyruvate dehydrogenase (E1), dihydrolipoic acid transacetylase (E2), dihydrolipoic acid dehydrogenase (E3) and E3 binding protein. E1 is a tetramer consisting of two units, pyruvate dehydrogenase E1 alpha subunit and E1 beta. E1 alpha subunit (PDHA1) plays an important role in activation and inactivation of PDHc, thus to be a key subunit.²⁷

Our previous studies have found that inhibition of PDHA1 expression promoted the stemness of prostate cancer cells and low level of PDHA1 protein expression was associated with poor prognosis in esophageal cancer clinical samples. To further investigate the effect of

PDHA1 KO on metabolism and biological characteristics of esophageal cancer cells, we established a stable KYSE450 PDHA1 KO cell line. CRISPR/Cas9 technology was used in this study, and the successfully deleted 34 bases in one allele of the exon 1 in *PDHA1* gene created a terminator code which disrupted the *PDHA1* gene expression and translation. The KO status of *PDHA1* gene was confirmed by DNA sequencing PCR product and its negative protein expression was verified by ICC and WB in our current study.

Compared with the parental cells, the basal OCR of PDHA1 KO cells was significantly reduced, while the basal ECAR was significantly increased, in addition to significantly decreased reserve respiratory capacity, verifying the Warburg status of the PDHA1 KO cells. In order to maintain metabolic balance, the KO cells increased the uptake of glucose and glutamine. These results suggest that the KYSE450 cells underwent metabolic reprogramming after PDHA1 KO.

ABCG2 is a member of ATP binding cassette transporter superfamily, and is expressed in a variety of cancer cells.²⁸ ABCG2 can transport a variety of chemotherapy drugs effectively, which is an important mechanism of cancer chemotherapy failure.^{29,30} It was reported that overexpression of ABCG2 in Eca109/ADM cells resulted in drug efflux, attributed to the development of esophageal cancer multidrug resistance (MDR).³¹ In our experiments,

we found that the KYSE450 PDHA1 KO cells showed resistance to both docetaxel and paclitaxel, at the same time the expression of ABCG2 was significantly increased, implying the potential role of increased ABCG2 expression in the chemoresistance of the PDHA1 KO cells.

In animal experiments, the volume and weight of xenograft tumor formed by the PDHA1 KO cells were higher than the control group, indicating that the enhanced proliferation ability of the PDHA1 KO cells in vivo, which was consistent with the in vitro results. In addition, the weight loss in the PDHA1 KO nude mice was more obvious, which may indicate that the PDHA1 KO cells consumed larger quantity of nutrients through a series of metabolic reprogramming activities including at least higher levels of glucose consumption and glutaminolysis. The phenomenon of weight loss in the PDHA1 KO mice may provide some clues for understanding the “cachexia” phenomenon of cancer patients.

Transcriptome analyses of the PDHA1 KO cells revealed a large panel of gene expression alterations. To evaluate the transcriptome reliability, a series of 9 highly up-regulated genes related to tumor malignant behaviors, including *CSF2*, *ANXA10*, *INHBA*, *IL1RL1*, *IL32*, *CCL20*, *IL1A*, *GPR31* and *BDKRB2* were further examined with RT-PCR.^{32–40} The RT-PCR results confirmed the transcriptome of these genes, implying the fidelity of the transcriptome. Further analysis of the genes significantly up- or down-regulated in this cell model may help to understand and reveal the molecular mechanism of Warburg effect.

P53 is an important tumor suppressor gene.^{41,42} In normal cells, p53 undergoes ubiquitination degradation by binding to the MDM2 (murine double minute 2), thereby maintaining a very low expression level.⁴³ Phosphorylation modification is an important post-translational modification of p53.⁴⁴ Phosphorylation of p53 inhibited the MDM2-p53 interaction, and enhanced stability of p53.⁴⁵ As a result, p53 is activated, then enters the nucleus and regulates downstream gene transcription, promoting cell cycle arrest and apoptosis. Ser15 is a common phosphorylation site of p53 (corresponding to Ser18 in mice). Studies have shown that phosphorylation of Ser15 can increase the stability of p53 and enhance its transcriptional activity.^{46–48} Decreased phosphorylation of p53 may lead to decreased chromosome stability, which may lead to escape apoptosis.^{49–51} It was confirmed in our current study that the phosphorylation of p53 (Ser15) in the KYSE450 PDHA1 KO cells was significantly lower than the control group. We speculate that the decreased p53

expression in functional state might lead the PDHA1 KO cells escape apoptosis, so that the PDHA1 KO cells obtained proliferation advantage.

Angiogenesis is not only for better nutrient delivery and oxygen supply, but also for further dissemination and distant metastasis. ANG2 is a member of Ang family and plays an important role in tumorigenesis and angiogenesis.^{52,53} When ANG2 acting together with VEGFA, they can interrupt the interaction between endothelial cells, promoting vascular germination and destabilize blood vessels, activate matrix degrading enzymes, including plasminogen activator (PAS) and matrix metalloproteinase (MMPs), allowing endothelial cells to migrate and germinate.^{54,55} Our study showed that MVD in the KO group increased, suggesting that the PDHA1 KO cells had enhanced angiogenesis. Transcriptional sequencing results showed that several genes related to angiogenesis were elevated in the PDHA1 KO cells, including *ANG1*, *ANG2*, *VEGFA*, *VEGFC* and *TGFB1*. Further detection of protein expression (WB) verified that the expressions of ANG2 and VEGFA in the PDHA1 KO cells were significantly increased. These indicated that the increased expression of Ang2 and VEGFA might be involved in the angiogenesis of the PDHA1 KO cells.

Conclusions

CRISPR/cas9 technology was applied in our study to successfully knock out the *PDHA1* gene in human esophageal squamous cancer cell line KYSE450, and a KYSE450 PDHA1 KO cell line was established. Compared with the parental cells, the PDHA1 KO cells exhibited Warburg effect with increased glucose and glutamine uptake. Further experiments suggested that PDHA1 KO cells were more proliferative both in vitro and in vivo, and significantly more migratory and chemotherapy-resistant in vitro. In addition, the PDHA1 KO cell-initiated xenograft tumors were reviewed highly vascularized. Collectively, our results prove that *PDHA1* gene KO in human ESCC cells results in metabolic reprogramming towards Warburg effect and increased cell malignancies, indicating strongly that the relationship between *PDHA1* gene activity and ESCC cell malignancy merit further studies.

Acknowledgment

This study was supported by the Radiumhospital Legat, Oslo, Norway and the Interdisciplinary Key Project of the First Affiliated Hospital of Zhengzhou University, Henan, China.

Disclosure

The authors report no conflicts of interest in this work.

References

- Salehinyia H, Otroshi O, Sadeghi-Gandomani H, et al. Esophageal cancer in the world: incidence, mortality and risk factors. *Biomed Res Ther.* 2018;5(7):2504–2517. doi:10.15419/bmrat.v5i7.460
- Liu Y, Xiong Z, Beasley A, D'Amico T, Chen XL. Personalized and targeted therapy of esophageal squamous cell carcinoma: an update. *Ann N Y Acad Sci.* 2016;1381(1):66–73. doi:10.1111/nyas.13144
- Boroughs LK, DeBerardinis RJ. Metabolic pathways promoting cancer cell survival and growth. *Nat Cell Biol.* 2015;17(4):351–359. doi:10.1038/ncb3124
- Pavlova NN, Thompson CB. The emerging hallmarks of cancer metabolism. *Cell Metab.* 2016;23(1):27–47. doi:10.1016/j.cmet.2015.12.006
- Gandhi N, Das GM. Metabolic reprogramming in breast cancer and its therapeutic implications. *Cells.* 2019;8:2. doi:10.3390/cells8020089
- Hanahan D, Weinberg RA. Hallmarks of cancer: the next generation. *Cell.* 2011;144(5):646–674. doi:10.1016/j.cell.2011.02.013
- Phan LM, Yeung SC, Lee MH. Cancer metabolic reprogramming: importance, main features, and potentials for precise targeted anticancer therapies. *Cancer Biol Med.* 2014;11(1):1–19. doi:10.7497/j.issn.2095-3941.2014.01.001
- Warburg O. On respiratory impairment in cancer cells. *Science.* 1956;124(3215):269–270.
- Warburg O. On the origin of cancer cells. *Science.* 1956;123(3191):309–314. doi:10.1126/science.123.3191.309
- Kim JW, Tchernyshyov I, Semenza GL, Dang CV. HIF-1-mediated expression of pyruvate dehydrogenase kinase: a metabolic switch required for cellular adaptation to hypoxia. *Cell Metab.* 2006;3(3):177–185. doi:10.1016/j.cmet.2006.02.002
- Kaplon J, Zheng L, Meissl K, et al. A key role for mitochondrial gatekeeper pyruvate dehydrogenase in oncogene-induced senescence. *Nature.* 2013;498(7452):109–112. doi:10.1038/nature12154
- Zabkiewicz J, Pearn L, Hills RK, et al. The PDK1 master kinase is over-expressed in acute myeloid leukemia and promotes PKC-mediated survival of leukemic blasts. *Haematologica.* 2014;99(5):858–864. doi:10.3324/haematol.2013.096487
- Qin L, Tian Y, Yu Z, et al. Targeting PDK1 with dichloroacetophenone to inhibit acute myeloid leukemia (AML) cell growth. *Oncotarget.* 2016;7(2):1395–1407. doi:10.18632/oncotarget.v7i2
- Zhong Y, Huang R, Li X, et al. Decreased expression of PDHE1alpha predicts worse clinical outcome in esophageal squamous cell carcinoma. *Anticancer Res.* 2015;35(10):5533–5538.
- Zhong Y, Li X, Ji Y, et al. Pyruvate dehydrogenase expression is negatively associated with cell stemness and worse clinical outcome in prostate cancers. *Oncotarget.* 2017;8(8):13344–13356. doi:10.18632/oncotarget.14527
- Gang BP, Dilda PJ, Hogg PJ, Blackburn AC. Targeting of two aspects of metabolism in breast cancer treatment. *Cancer Biol Ther.* 2014;15(11):1533–1541. doi:10.4161/15384047.2014.955992
- Shroff EH, Eberlin LS, Dang VM, et al. MYC oncogene overexpression drives renal cell carcinoma in a mouse model through glutamine metabolism. *Proc Natl Acad Sci U S A.* 2015;112(21):6539–6544. doi:10.1073/pnas.1507228112
- Clavell LA, Gelber RD, Cohen HJ, et al. Four-agent induction and intensive asparaginase therapy for treatment of childhood acute lymphoblastic leukemia. *N Engl J Med.* 1986;315(11):657–663. doi:10.1056/NEJM198609113151101
- Folmes CD, Dzeja PP, Nelson TJ, Terzic A. Metabolic plasticity in stem cell homeostasis and differentiation. *Cell Stem Cell.* 2012;11(5):596–606. doi:10.1016/j.stem.2012.10.002
- Folmes CD, Martinez-Fernandez A, Faustino RS, et al. Nuclear reprogramming with c-Myc potentiates glycolytic capacity of derived induced pluripotent stem cells. *J Cardiovasc Transl Res.* 2013;6(1):10–21. doi:10.1007/s12265-012-9431-2
- Kida YS, Kawamura T, Wei Z, et al. ERRs mediate a metabolic switch required for somatic cell reprogramming to pluripotency. *Cell Stem Cell.* 2015;16(5):547–555. doi:10.1016/j.stem.2015.03.001
- Moussaieff A, Rouleau M, Kitsberg D, et al. Glycolysis-mediated changes in acetyl-CoA and histone acetylation control the early differentiation of embryonic stem cells. *Cell Metab.* 2015;21(3):392–402. doi:10.1016/j.cmet.2015.02.002
- Riester M, Xu Q, Moreira A, Zheng J, Michor F, Downey RJ. The Warburg effect: persistence of stem-cell metabolism in cancers as a failure of differentiation. *Ann Oncol.* 2018;29(1):264–270. doi:10.1093/annonc/mdx645
- Cui J, Shi M, Xie D, et al. FOXM1 promotes the warburg effect and pancreatic cancer progression via transactivation of LDHA expression. *Clin Cancer Res.* 2014;20(10):2595–2606. doi:10.1158/1078-0432.CCR-13-2407
- Nie H, Li J, Yang XM, et al. Mineralocorticoid receptor suppresses cancer progression and the Warburg effect by modulating the miR-338-3p-PKLR axis in hepatocellular carcinoma. *Hepatology.* 2015;62(4):1145–1159. doi:10.1002/hep.27940
- Icard P, Shulman S, Farhat D, Steyaert JM, Alifano M, Lincet H. How the Warburg effect supports aggressiveness and drug resistance of cancer cells? *Drug Resist Updat.* 2018;38:1–11. doi:10.1016/j.drup.2018.03.001
- Patel KP, O'Brien TW, Subramony SH, Shuster J, Stacpoole PW. The spectrum of pyruvate dehydrogenase complex deficiency: clinical, biochemical and genetic features in 371 patients. *Mol Genet Metab.* 2012;106(3):385–394. doi:10.1016/j.ymgme.2012.03.017
- Mo W, Zhang JT. Human ABCG2: structure, function, and its role in multidrug resistance. *Int J Biochem Mol Biol.* 2012;3(1):1–27.
- Mao Q, Unadkat JD. Role of the breast cancer resistance protein (BCRP/ABCG2) in drug transport—an update. *Aaps J.* 2015;17(1):65–82. doi:10.1208/s12248-014-9668-6
- Westover D, Li F. New trends for overcoming ABCG2/BCRP-mediated resistance to cancer therapies. *J Exp Clin Cancer Res.* 2015;34:159. doi:10.1186/s13046-015-0275-x
- Liu L, Zuo LF, Guo JW. ABCG2 gene amplification and expression in esophageal cancer cells with acquired adriamycin resistance. *Mol Med Rep.* 2014;9(4):1299–1304. doi:10.3892/mmr.2014.1949
- Montana V, Sontheimer H. Bradykinin promotes the chemotactic invasion of primary brain tumors. *J Neurosci.* 2011;31(13):4858–4867. doi:10.1523/JNEUROSCI.3825.2011
- Lee HY, Li CC, Huang CN, et al. INHBA overexpression indicates poor prognosis in urothelial carcinoma of urinary bladder and upper tract. *J Surg Oncol.* 2015;111(4):414–422. doi:10.1002/jso.23836
- Leon X, Bothe C, Garcia J, et al. Expression of IL-1alpha correlates with distant metastasis in patients with head and neck squamous cell carcinoma. *Oncotarget.* 2015;6(35):37398–37409. doi:10.18632/oncotarget.6054
- Erturk K, Tastekin D, Serilmez M, Bilgin E, Bozbey HU, Vatansever S. Clinical significance of serum interleukin-29, interleukin-32, and tumor necrosis factor alpha levels in patients with gastric cancer. *Tumour Biol.* 2016;37(1):405–412. doi:10.1007/s13277-015-3829-9
- Lee YY, Wu WJ, Huang CN, et al. CSF2 overexpression is associated with STAT5 phosphorylation and poor prognosis in patients with urothelial carcinoma. *J Cancer.* 2016;7(6):711–721. doi:10.7150/jca.14281
- Chen W, Qin Y, Wang D, et al. CCL20 triggered by chemotherapy hinders the therapeutic efficacy of breast cancer. *PLoS Biol.* 2018;16(7):e2005869. doi:10.1371/journal.pbio.2005869
- Rong YM, Huang XM, Fan DJ, et al. Overexpression of G protein-coupled receptor 31 as a poor prognosticator in human colorectal cancer. *World J Gastroenterol.* 2018;24(41):4679–4690. doi:10.3748/wjg.v24.i41.4679

39. Wang J, Zhao S, Wang F, Wang J, Zhang Y. Prognostic Significance of increased expression of annexin A10 (ANXA10) in serous epithelial ovarian cancer. *Med Sci Monit.* 2019;25:5666–5673. doi:10.12659/MSM.915911
40. Wang Y, Richter L, Becker M, Amador C, Hyde RK. IL1RL1 is dynamically expressed on Cbfb-MYH11(+) leukemia stem cells and promotes cell survival. *Sci Rep.* 2019;9(1):1729. doi:10.1038/s41598-018-38408-3
41. Vogelstein B, Kinzler KW. p53 function and dysfunction. *Cell.* 1992;70(4):523–526. doi:10.1016/0092-8674(92)90421-8
42. Levine AJ. p53, the cellular gatekeeper for growth and division. *Cell.* 1997;88(3):323–331. doi:10.1016/S0092-8674(00)81871-1
43. Prives C. Signaling to p53: breaking the MDM2-p53 circuit. *Cell.* 1998;95(1):5–8. doi:10.1016/S0092-8674(00)81774-2
44. Bode AM, Dong Z. Post-translational modification of p53 in tumorigenesis. *Nat Rev Cancer.* 2004;4(10):793–805. doi:10.1038/nrc1455
45. Moll UM, Petrenko O. The MDM2-p53 interaction. *Mol Cancer Res.* 2003;1(14):1001–1008.
46. Khanna KK, Keating KE, Kozlov S, et al. ATM associates with and phosphorylates p53: mapping the region of interaction. *Nat Genet.* 1998;20(4):398–400. doi:10.1038/3882
47. Ashcroft M, Vousden KH. Regulation of p53 stability. *Oncogene.* 1999;18(53):7637–7643. doi:10.1038/sj.onc.1203012
48. Tibbetts RS, Brumbaugh KM, Williams JM, et al. A role for ATR in the DNA damage-induced phosphorylation of p53. *Genes Dev.* 1999;13(2):152–157. doi:10.1101/gad.13.2.152
49. MacPherson D, Kim J, Kim T, et al. Defective apoptosis and B-cell lymphomas in mice with p53 point mutation at Ser 23. *Embo J.* 2004;23(18):3689–3699. doi:10.1038/sj.emboj.7600363
50. Sluss HK, Armata H, Gallant J, Jones SN. Phosphorylation of serine 18 regulates distinct p53 functions in mice. *Mol Cell Biol.* 2004;24(3):976–984. doi:10.1128/MCB.24.3.976-984.2004
51. Chao C, Herr D, Chun J, Xu Y. Ser18 and 23 phosphorylation is required for p53-dependent apoptosis and tumor suppression. *Embo J.* 2006;25(11):2615–2622. doi:10.1038/sj.emboj.7601167
52. Hu B, Cheng SY. Angiopoietin-2: development of inhibitors for cancer therapy. *Curr Oncol Rep.* 2009;11(2):111–116. doi:10.1007/s11912-009-0017-3
53. Fagiani E, Christofori G. Angiopoietins in angiogenesis. *Cancer Lett.* 2013;328(1):18–26. doi:10.1016/j.canlet.2012.08.018
54. Lobov IB, Brooks PC, Lang RA. Angiopoietin-2 displays VEGF-dependent modulation of capillary structure and endothelial cell survival in vivo. *Proc Natl Acad Sci U S A.* 2002;99(17):11205–11210. doi:10.1073/pnas.172161899
55. Saharinen P, Eklund L, Pulkki K, Bono P, VEGF AK. and angiopoietin signaling in tumor angiogenesis and metastasis. *Trends Mol Med.* 2011;17(7):347–362. doi:10.1016/j.molmed.2011.01.015

OncoTargets and Therapy

Dovepress

Publish your work in this journal

OncoTargets and Therapy is an international, peer-reviewed, open access journal focusing on the pathological basis of all cancers, potential targets for therapy and treatment protocols employed to improve the management of cancer patients. The journal also focuses on the impact of management programs and new therapeutic

agents and protocols on patient perspectives such as quality of life, adherence and satisfaction. The manuscript management system is completely online and includes a very quick and fair peer-review system, which is all easy to use. Visit <http://www.dovepress.com/testimonials.php> to read real quotes from published authors.

Submit your manuscript here: <https://www.dovepress.com/oncotargets-and-therapy-journal>